Published online 13 February 2018 *Nucleic Acids Research, 2018, Vol. 46, No. 6* **2945–2955**
doi: 10.1093/nar/gky076

DNA mismatch repair and oligonucleotide end-protection promote base-pair substitution distal from a CRISPR/Cas9-induced DNA break

Tim Harmsen[1], Sjoerd Klaasen[1], Henri van de Vrugt[1,2] and Hein te Riele[1,*]

[1]Division of Tumor Biology and Immunology, The Netherlands Cancer Institute, Plesmanlaan 121, 1066 CX Amsterdam, The Netherlands and [2]Department of Clinical Genetics, VU University Medical Center, Van der Boechorststraat 7, 1081 BT Amsterdam, The Netherlands

Received July 7, 2017; Revised January 19, 2018; Editorial Decision January 24, 2018; Accepted January 25, 2018

ABSTRACT

Single-stranded oligodeoxyribonucleotide (ssODN)-mediated repair of CRISPR/Cas9-induced DNA double-strand breaks (DSB) can effectively be used to introduce small genomic alterations in a defined locus. Here, we reveal DNA mismatch repair (MMR) activity is crucial for efficient nucleotide substitution distal from the Cas9-induced DNA break when the substitution is instructed by the 3′ half of the ssODN. Furthermore, protecting the ssODN 3′ end with phosphorothioate linkages enhances MMR-dependent gene editing events. Our findings can be exploited to optimize efficiencies of nucleotide substitutions distal from the DSB and imply that oligonucleotide-mediated gene editing is effectuated by templated break repair.

INTRODUCTION

Protocols for introducing small genomic sequence alterations are of great value to investigate the function of specific protein residues in their endogenous context, or assess the pathogenicity of variants of uncertain significance of disease-related genes. The most efficient protocols take advantage of the site-specific endonuclease *Streptococcus pyogenes* Type II Cas9 (*Sp*Cas9) (1–3). *Sp*Cas9 is directed to a specific genomic locus by a 'guide RNA' (gRNA) containing 20 nucleotides (nt) identical to a region of the target locus that is called the 'protospacer' and is adjacent to an 'NGG' triplet, the 'protospacer adjacent motif' (PAM). Subsequent activation of the nuclease domains of *Sp*Cas9 results in a DNA double-strand break (DSB) three basepairs upstream of the PAM (1). By supplying short (60–120 nt) single-stranded oligodeoxyribonucleotides (ssODN) that can be utilized by cellular homology-dependent DSB repair processes, tailored sequence alterations can be engineered (4,5). Based on early work in yeast, two models have been proposed to describe ssODN-mediated DSB repair, that were referred to as the 'bridge model' (Supplementary Figure S1a) and the 'template model' (Supplementary Figure S1b) (6). The two models differ by the initial processing of the broken DNA ends: unwinding in case of the bridge model and end-resection in case of the template model. The bridge model comprises the following steps: (i) unwinding of the two genomic DNA (gDNA) ends produced by the DSB; (ii) annealing of the ssODN to the 3′ and 5′ ends of the same gDNA strand, ('bridging' the gap); (iii) reannealing of the gDNA strands and flap formation of the 5′ and 3′ ends of the other gDNA strand; (iv) flap removal followed by gap-filling and ligation. DSB repair by this mechanism would lead to integration of the oligonucleotide into the genome. The template model shares steps with canonical homology directed DSB repair (7): (i) resection of the 5′ gDNA ends; (ii) capturing of the ssODN by one 3′ gDNA end; (iii) elongation of this genomic 3′ end using the ssODN as template; (iv) annealing of the gDNA ends, followed by (v) gap-filling and ligation. In the bridge model, mutations encoded within both the 5′ or 3′ annealing arms of the ssODN will result in DNA mismatches. The template model predicts that only mutations encoded within the 3′ half of the ssODN will result in mismatched DNA, as this is the only region that can anneal to a 3′ gDNA end. More recently, models reminiscent of the bridge and template models have been proposed for ssODN-mediated repair of DNA nicks, dependent on the polarity of the ssODN with respect to the nicked strand (8–10). A ssODN complementary to the intact strand ('cI donor') would effectuate repair and concomitant gene modification via 'single-strand DNA incorporation' (ssDI), while an ssODN complementary to the nicked strand ('cN donor') would serve as a template for DNA synthesis in a process referred to as 'synthesis-dependent strand annealing' (SDSA) (10), or perhaps more accurately 'annealing-driven strand synthesis' (ADSS) (9). Subsequently, evidence was obtained for the latter pathway to dominate ssODN-mediated repair of a DNA double-stranded break (10).

*To whom correspondence should be addressed. Tel: +31 20 512 2084; Fax: +31 20 512 2057; Email: h.t.riele@nki.nl

In traditional gene targeting experiments, small differences between gDNA and exogenous DNA templates elicit DNA mismatch repair (MMR) activity that suppresses the gene modification reaction (11). MMR also counteracts subtle gene modification in protocols that make use of short single-stranded DNA oligonucleotides *without* the assistance of nucleases (12–16). Most recently, indications were reported for MMR-dependent anti-recombination during ssODN-mediated repair of DNA nicks (10). The mechanism of MMR-directed anti-recombination is not fully understood but likely involves dissociation of mismatched recombination intermediates, either by a canonical MMR reaction or a separate 'heteroduplex rejection' activity of MMR. Here, we investigated the role of MMR during ssODN-mediated repair of a CRISPR/Cas9-induced DSB.

MATERIALS AND METHODS

Plasmid vectors and oligonucleotides

pX330-U6-Chimeric_BB-CBh-hSpCas9 was a gift from Dr Feng Zhang (Addgene plasmid # 42230). A puromycin-resistance gene (see Supplementary Note 1) was cloned into the XhoI and ClaI sites of px330, yielding px330.pgkpur.

Oligonucleotides encoding gRNAs targeting the *GFP* reporter, *Msh2*, *Msh6* and *Mlh1* were designed and cloned as described (2). All mutating oligonucleotides were synthesized and purified by Sigma-Aldrich at 25 nmol synthesis scale followed by desalting. See Supplementary Table S1 for the sequences of all mutating oligonucleotides used in this study.

Part of the sequence of the *GFP* reporter showing the promoter, the *GFP* coding sequence and the SV40 polyadenylation signal is shown in Supplementary Note 2.

Mouse ES cell culture on MEFs

Mouse ES cells were cultured as described (12). Briefly, mouse ES cells were cultured on irradiated C57Bl/6-derived mouse embryonic fibroblasts in GMEM-BHK21 (Life Technologies) + 9% ES cell certified serum (Hiclone) with 1 × pyruvate, 1 × non-essential amino acids, 0.1 μM β-mercaptoethanol and mouse recombinant leukemia inhibitor factor, referred to as 'complete medium'.

Mouse ES cell GFP reporter lines

Msh2$^{+/+}$ and *Msh2*$^{-/-}$ ESCs containing a single copy of the GFP reporter inserted into the *Rosa26* locus were obtained from and created according to Aarts *et al.* (13).

Feeder-free ES cell culture on gelatin, HDR-mediated base pair substitution by CRISPR/Cas9

Prior to transfections, cells were grown in feeder-free conditions as described (12). For a typical transfection, mouse ES cells growing on feeders were trypsinized using phosphate-buffered saline + 5% Chicken serum (Gibco) + 0.05% Trypsin ethylenediaminetetraacetic acid (Life technologies) and seeded in 60% BRL medium (150 ml Buffalo Rat Liver conditioned complete medium + 100 ml complete medium + 2 mM Glutamax) at 5 × 10^4 (unless otherwise indicated) cells/well on gelatin-coated 6 wells or 10^4 cells per 24 well. Two days after seeding, medium was replaced by fresh 60% BRL medium. Within 1 h after refreshing, a DNA solution was prepared by mixing 0.25 μg CRISPR/Cas9 vector + 2.25 μg homology-directed repair (HDR) oligonucleotide template in 250 μl optiMEM (Gibco), unless otherwise indicated, for a 6 well or 0.1 μg CRISPR/Cas9 vector + 450 ng oligonucleotide template for a 24 well. Either 7.5 μl Fugene 6 (Promega) or 6.25 μl TransIT LT1 (Mirus) was added and the solution was mixed by pipetting. After 15–20 min incubation at room temperature, DNA–Fugene 6 or DNA–LT1 complexes were added to cells. Cells were incubated at 37°C and 5% CO_2. After 15 to 24 h incubation, cells were reseeded 1/5 in 60% BRL medium containing 3.6 μg/ml puromycin in a 6 well. Two days after reseeding, medium was refreshed with 60% BRL without puromycin. Two days later, cells were trypsinized and assayed by flow cytometry.

Flow cytometry measurement of fraction of GFP positive cells

The percentage of GFP positive cells was determined by flow cytometry on a Cyan ADP flow cytometer (Dako Cytomation). Propidium Iodide was used to exclude dead cells.

Data was analyzed using summit software 4.301 or 6.2. The percentage of GFP-positive cells was determined in the live, single-cell population. Our gating strategies yielded 0.01% of GFP-positive cells in an untransfected sample in a typical experiment.

Generation of Mlh1 knockout mESC cells

To generate *Mlh1* deficient mESCs, two separate transfections of MMR-proficient GFP-reporter cells were performed with px330.pgkpur vector expressing gRNAs with a protospacer sequence: **G**ATCATCTCTTTGATAGCAT (2019) and **G**GGCAGCTGATTCTACCAGA (2017), targeting exon 1 and 10, respectively. After puromycin selection, colonies were picked and cultured. Bold indicates extra G for optimal expression.

Mlh1 fragments of puromycin resistant clones obtained with CRISPRs 2019 and 2017 were amplified by polymerase chain reaction (PCR) using primers HH190: CGCTTGACTGGCATTCATG and HH191: CATAATGGGAAACCAGCCTG (clones modified with CRISPR 2019) or primers $MLH1_{fw}$ and $MLH1_{rev}$ (see below) (clones modified with CRISPR 2017). PCR products were analyzed by Sanger sequencing using primers HH190 and $MLH1_{fw}$ and Big Dye Terminator V3.1 (ThermoFisher), according to manufacturer's instruction. MLH1 protein levels were determined by western blotting. Methylating agent sensitivity was determined by seeding 10^3 cells on a gelatin-coated 6-well dish in 60% BRL medium containing 250 nM 6-thioguanine. Seven days later, medium was replaced with 60% BRL medium and four days later, cells were fixed with Leishman's solution and colonies were counted.

MMR-proficient and -deficient GFP reporter Hap1 cells

Hap1 cells were cultured as described by Carette *et al.* (17).

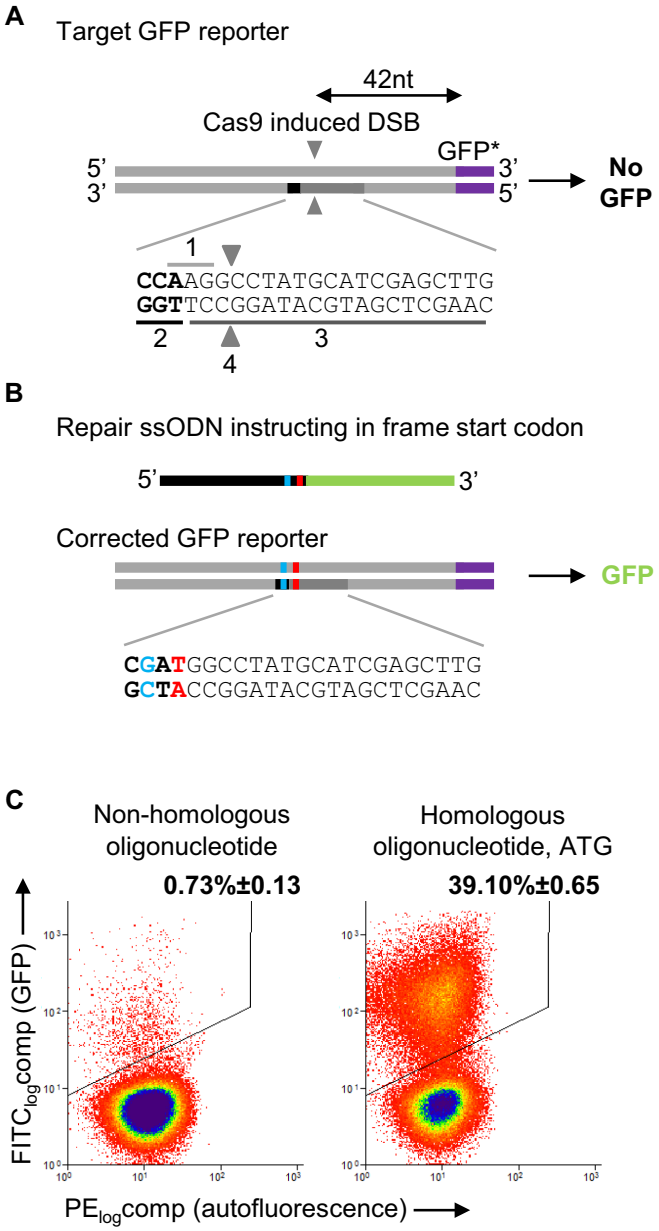

Figure 1. A GFP reporter system to study CRISPR/Cas9-mediated nucleotide substitutions. (**A**). Schematic representation of the GFP reporter with part of the sequence. Gray lines: double-stranded DNA upstream of the GFP open reading frame (purple lines) without start codon. Black rectangle: 5′-NGG PAM. Dark gray line: protospacer region. Dark gray triangles: site of the DSB. The sequence shows: (1) in frame AAG triplet, (2) the PAM, (3) the protospacer sequence, (4) the predicted location of the Cas9-induced DSB. A single copy of the GFP reporter was inserted into the *Rosa26* locus. (**B**) Strategy to activate GFP by substituting AAG for ATG. Black and green parts in the repair ssODN: 5′ half and 3′ half separated by the projected Cas9-induced DSB. Red rectangle: generation of a start codon by AAG to ATG substitution; blue rectangle: PAM disruption by TGG to TCG substitution. (**C**) Appearance of GFP-positive cells obtained after selection for uptake of the CRISPR/Cas9 vector using puromycin. The 120 nt single-stranded homologous oligonucleotide dictates concomitant AAG>ATG conversion and CCA>CGA PAM disruption (Supplementary Table S1). Percentages of GFP-positive cells are indicated ($n = 8$; ± SEM; $P < 0.0001$).

Briefly, cells were cultured in Iscove's Modified Dulbecco's Medium (IMDM; Life Technologies) supplemented with foetal calf serum (FCS) and penicillin/streptomycin. *GFP*-reporter bearing Hap1 cells were created by transfecting the cells with a human *EF1a* promoter-driven mutated *GFP* vector (full sequence in Supplementary Note 3), flanked by *ROSA26* homology arms and the px330.pgkpuro vector with a gRNA targeting the human *ROSA26* locus (18) with the protospacer sequence: GGTGCAGCAAGGGTCTCAAA. Two days after transfection, Hap1 cells were reseeded at low density and cultured in 2 mM histidinol until the appearance of histidinol-resistant colonies, which were manually dissociated. Subsequently, one haploid clone was selected carrying the *GFP* reporter (data not shown). This clone was rendered DNA MMR-deficient by transfection of px330.pgkpur vectors containing one of the following guides: *MSH2–1:* GTCGAAAAGGCGCACTGTGG, *MSH2–2:* GAACTTCAACACAAGCATGCC, *MLH1*: GAAGTACATCCTGGAGGAAT and subsequent selection with 6-thioguanine at a concentration of 1.5 μM for ∼10 days. Four different 6-thioguanine-resistant clones were selected, that showed frameshifting deletions in the targeted MMR genes. MMR-proficient and -deficient Hap1 cells were transfected with the same vector and ssODNs used for the mESCs. Eight days after transfection, cells were analyzed by flow cytometry. Data was max-normalized and averaged over the four different MMR-deficient clones to generate the data-points of MMR-deficient Hap1 cells shown in Figure 2G.

Processing of the data and statistics

Percentages of GFP-positive cells shown in Figures 1 and 2 were obtained in different experiments on different days, with two independent transfections used to generate data for each day. To compile the data into one figure, GFP percentages in an experiment were multiplied by factor (A/B), A being the average positive control (ssODN sense 90NT +ATG+PAM) value of all experiments with MMR-proficient or -deficient cells, B being the positive control value in a given experiment. Then, background GFP signal was subtracted. This signal was determined in MMR-proficient and -deficient cells transfected with an oligonucleotide containing only a PAM disrupting mutation (sense 90NT +PAM). Generally, it was in the order of 1–2%. Error bars denote the standard error of mean. Two-tailed, unpaired *t*-tests were performed with Graphpad Prism software version 6 for Windows to determine significance. **** indicate $P < 0.0001$, *** $P < 0.001$, ** $P < 0.01$, * $P < 0.05$. Confidence intervals were calculated using Microsoft Excel 2013 and given in Supplementary Note 4.

Msh2/Msh6/Mlh1 RFLP analysis

MMR-proficient or -deficient mESCs were transfected with px330.pgkpuro vector with gRNAs against *Msh2*, *Msh6* or *Mlh1* (protospacer sequences *Msh2*: GGATCAGTTCTCCAATCTCG; *Msh6*: GTTGGGGAAGAAGCTGTACA; *Mlh1*: GGGCAGCTGATTCTACCAGA) and a 120 nt ssODN template as described above.

On day 7 after transfection, gDNA was isolated and used to amplify the modified locus by PCR using the following

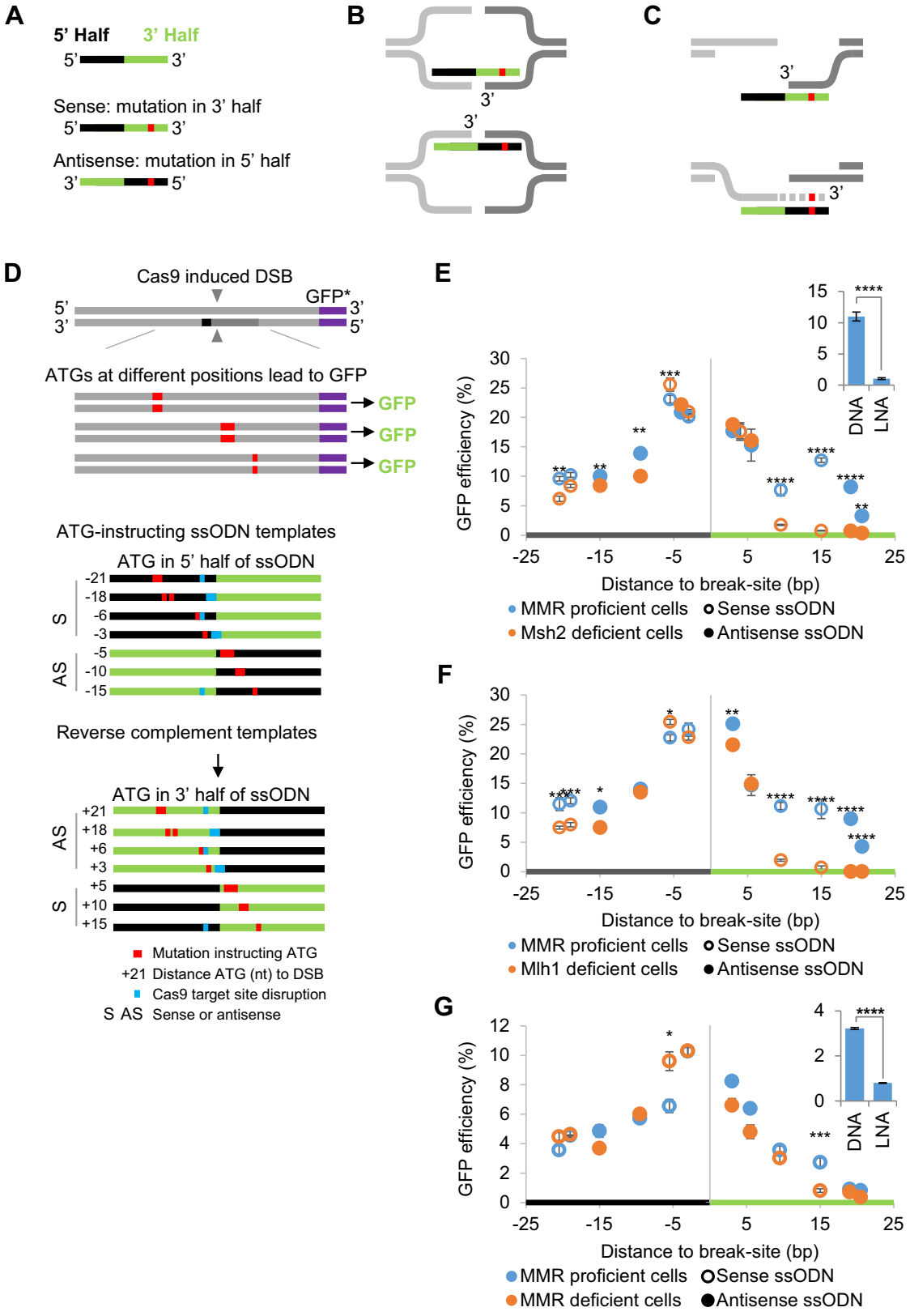

Figure 2. Introduction efficiency of break-distal substitutions. (**A**) 5′ and 3′ halves of an ssODN are indicated in black and green, respectively. A mutation (red rectangle) instructed by the 3′ half of a sense ssODN is instructed by the 5′ half of the complementary antisense ssODN, and *vice versa*. (**B**) Annealing of sense and antisense ssODNs to chromosomal ends in the 'bridge' model. Mutating nucleotides in both, the 5′ and 3′ half create a mismatch. (**C**) Annealing of sense and antisense ssODNs to chromosomal ends in the 'template' model. Only mutating nucleotides in the 3′ half create a mismatch. (**D**) Activation of the GFP reporter. A break is introduced in the GFP reporter sequence by Cas9 (as in Figure 1A). In-frame ATGs are instructed by seven sense and seven

primer pairs: $MSH6_{fw}$: ACACGCCTTCGGATTGG; $MSH6_{rev}$: GGGTTCAGCCTCGCTCC; $MSH2_{fw}$: TCTTTCTCAGTTTGAA GACATCC; $MSH2_{rev}$: GGGGTATTTTACATGAAGG; $MLH1_{fw}$: CTTTCAGAGCAGTGACAAGG; $MLH1_{rev}$: GGGCTTTTGTTC CTGGG.

The following PCR program was used to amplify the respective loci: 2′ 94°C; 37× (30′ 94°C; 30′ tm; $T_{elongation}$ 72°C); 5′ at 72°C; incubation at 4°C, with tm 56°C for *Mlh1*, 53.8°C for *Msh2* and 60°C for *Msh6*. $T_{elongation}$ was 30′ for *Msh6* and *Mlh1*, 40′ for *Msh2*. The PCRs were done in a final volume of 150 μl for each sample. PCR products were purified by precipitation (addition of 0.1 volume of 3M NaAc, pH 5.0 and 0.7 volumes of isopropanol, followed by 30′ centrifugation at 4°C), washing of the pellets in 70% EtOH, drying and suspension in an appropriate volume of TE buffer (typically 50 μl).

The 1 μl of purified PCR product was digested by addition of 2× restriction mix, containing 0.1 μl of the appropriate restriction enzyme, 0.2 μl 10× restriction enzyme buffer and 0.7 μl MQ H_2O. This reaction was incubated for 2 h and 45 min at 37°C on a Peltier Thermal Cycler (PTC-100; MJ Research).

The products of the restriction enzyme reaction were analyzed on Caliper Labchip GX ($n = 3$) using the DNA high sensitivity protocol to quantify digestion products and hence the efficacy of base-pair substitution. Introduction efficiency was calculated as [(amount of cleaved DNA)/(amount of cleaved DNA + amount of uncleaved DNA)] × 100%.

RESULTS

To study the impact of MMR on CRISPR/Cas9-assisted oligonucleotide-mediated gene editing, we used mouse embryonic stem cells (ESCs), engineered to carry a single copy of a disabled green fluorescent protein gene (*GFP*) lacking the start codon (19). Base-pair substitutions creating in-frame start codons upstream of the *GFP* coding sequence result in green fluorescence. A puromycin-selectable vector was established that expresses *Sp*Cas9 and a gRNA to create a DSB in the reporter gene one nucleotide downstream of an in-frame AAG triplet (Figure 1A). Upon introduction of the vector alone, ±1% of puromycin-resistant ESCs became GFP-positive indicative for the creation of an in-frame start codon following error-prone DSB repair by non- or micro-homology mediated end joining. The addition of a 120 nt ssODN designed to direct conversion of the in-frame AAG triplet close to the Cas9-induced break into a start codon raised the frequency of GFP-positive cells to 39% (Figure 1B and C). Thus, this reporter system provides a convenient readout for homology directed DSB repair. Note that we added an additional mutation to simultaneously disrupt the PAM sequence in order to prevent re-cutting by Cas9 and loss of gene correction events (20).

We used this system to assess the feasibility and efficiency of base-pair substitution at different distances from the break, taking advantage of the fact that GFP can be produced upon generation of any in-frame start codon (ATG) upstream of the open reading frame. Substitutions can be generated by sense or anti-sense ssODNs, each divided in a 5′ half and a 3′ half by the projected break site; when a given mutating nucleotide is present in the 3′ half of a sense ssODN, it is in the 5′ part of the complementary antisense ssODN and *vice versa* (Figure 2A). When gDNA ends anneal to these ssODNs, the bridge model predicts the formation of a mismatch with both types of ssODN (Figure 2B). In contrast, the template model only generates a mismatch when the mutation is instructed by the 3′ half of the ssODN (**2c**). To study the consequences of these mismatches, we measured substitution efficiencies in MMR-proficient and -deficient ESCs.

We designed seven pairs of 90 nt sense and corresponding antisense ssODNs encoding start-codon-creating substitutions at various distances from the DSB site within either the 5′ or the 3′ half of the ssODN (Figure 2D). To avoid re-cutting (and hence loss of GFP-activating correction events), we took care that the Cas9 recognition site became simultaneously disrupted, either because the mutation affected the protospacer region by more than 1 base pair (bp), or by adding a PAM-disrupting mutation (20). We first determined the efficiency of *GFP* correction in MMR-deficient ESCs carrying a disruption in the key MMR gene *Msh2* (Figure 2E, orange symbols). Break proximal substitutions—within 6 nt from the break—were achieved at frequencies of 15–21%, 3′ half instructed substitutions being only slightly less effective than 5′ half instructed substitutions. However, at distances larger than 9 nt, the side with respect to the DSB had a strong impact: whereas ATGs instructed by the 5′ half of the ssODN were introduced at ef-

antisense ssODNs either within the 5′ half (black) or within the 3′ half (green). Each ssODN instructs a start codon (schematically represented in red) at a different distance from the break (indicated by the number shown on the left of each ssODN; a negative number indicates the ATG is instructed by the 5′ half, a positive number indicates the ATG is instructed by the 3′ half). To avoid re-cutting of the target site after ssODN-mediated repair, additional Cas9 target site disrupting mutations were included if the ATG creating heterology modified <2 bases of the protospacer. Blue rectangle in ssODN pairs +3/−3: a 2 bp substitution disrupting the protospacer; blue rectangles in ssODN pairs +21/−21, −15/+15, +6/−6, are PAM disrupting mutations, in case of the latter pair it is also part of the start codon. In case of the +18/−18 pair, a 2 bp deletion was necessary to bring the ATG in frame, concomitantly disrupting the protospacer. The exact ssODN sequences can be found in Supplementary Table S1. (**E**) Introduction efficiency of ATGs with the seven different sense (open circles) and seven antisense ssODNs (closed circles) from (**D**) in MMR-proficient (blue symbols) and *Msh2*-deficient (red symbols) murine embryonic stem cells (mESCs), plotted versus the distance of the ATG to the projected DSB ($n = 6$; error bars indicate SEM; *P*-values determined between MMR-proficient and -deficient samples: $^{****}P < 0.0001$, $^{***}P < 0.001$, $^{**}P < 0.01$). Insert: introduction efficiency of the ATG-creating mutation at position +15 in the 3′ half of the ssODN in MMR-proficient cells, present as a DNA base or an LNA base ($n = 4$; error bars indicate SEM. $^{****}P < 0.0001$). Supplementary Figure S2a and b show example flow cytometry plots of DNA MMR-proficient and -deficient cells, respectively, after introduction of a break-proximal and a 3′ half break-distal mutation. (**F**) Introduction efficiency of ATGs with six different sense (open circles) and antisense (closed circles) from (**D**) in MMR-proficient (blue symbols, $n = 2$) and *Mlh1*-deficient (red symbols, $n = 10$) mESCs. (**G**) Introduction efficiency of ATGs with six different sense (open circles) and antisense (closed circles) from (**D**) in MMR-proficient (blue symbols, $n = 2$) and MMR-deficient (red symbols, $n = 8$) human Hap1 cells. The data for MMR-deficient Hap1 cells were obtained by averaging the results obtained in four different clones. $^{*}P < 0.05$, $^{***}P < 0.001$. Insert: instructing a mutation at position +15 with a DNA or LNA base in MMR-proficient Hap1 cells, as in (**E**), *insert*. $^{****}P < 0.0001$.

ficiencies of 6–10%, ATGs instructed by the 3′ half of the ssODN were hardly obtained.

It is possible that the low efficiency of break-distal substitutions instructed by the 3′ half of the ssODN was due to 3′ end degradation of the ssODN. However, when we performed this experiment in MMR-proficient ESCs, a different result was obtained (Figure 2E, blue symbols). Base-pair substitutions in close proximity of the break and 5′ half encoded distal substitutions were generated with similar efficiencies as in *Msh2*-deficient cells. Strikingly, the introduction efficiencies of distal mutations by the 3′ half of the ssODN were up to 17-fold higher in MMR-proficient versus *Msh2*-deficient cells, indicating that MSH2 is vital to transfer mutations from the 3′ half of the ssODN to the gDNA. To confirm that in these cases recognition of the mismatch by MSH2 was critical to achieve base-pair substitution, we made use of the observation that a mismatch containing a locked nucleic acid (LNA) is not recognized by MSH2 (21). Indeed, when the ATG-creating nucleotide at position +15 in the ssODN was an LNA, the frequency of green fluorescent MMR-proficient cells dropped to background level (Figure 2E, insert). These results unexpectedly demonstrate that MSH2 is critical for effective substitution of nucleotides instructed by the 3′ half of the oligonucleotide.

MSH2 together with its partner MSH6 recognizes and binds mismatches in DNA. Subsequent MMR requires recruitment of a second complex, MLH1/PMS2, which is essential for excision of the error-containing DNA strand (22). To investigate whether break-distal nucleotide substitution relies on MSH2 mismatch binding activity only or also on downstream MMR events, we generated *Mlh1*-deficient *GFP* reporter mESCs (Supplementary Figure S3). In these cells, we noted a small but reproducibly decreased substitution efficiency of break-proximal base pairs (Supplementary Figure S4), indicative for a reduced HDR efficiency in these cells. To better compare the efficiencies of 5′ and 3′ break distal base-pair substitution, we normalized the values obtained in *Mlh1*-deficient cells to those of MMR-proficient cells by equalizing the mean substitution efficiencies of break-proximal mutations (Figure 2F). We found that introduction of break-distal mutations instructed by the 3′ half of the ssODN was suppressed up to 15-fold in *Mlh1*-deficient ESCs. This demonstrates that the core DNA MMR pathway is important for the break-distal introduction of 3′-half-instructed mutations during ssODN-mediated DSB repair.

To investigate whether DNA MMR also promotes induction of 3′-half-instructed mutations in human cell lines, we generated wild-type and *MSH2*- or *MLH1*-defective human Hap1 cells carrying the *GFP* reporter sequence. MMR-defective HAP1 cells were obtained by CRISPR/Cas9-mediated gene disruption and subsequent selection for resistance to 6-thioguanine, a hallmark of MMR deficiency. 6TG-resistant colonies invariably showed frameshifting deletions in *MSH2* or *MLH1* (not shown). We compared the introduction efficiency of ATGs at various distances from the DSB in MMR-proficient and -deficient cells. We observed that introduction of mutations at a distance of 10 nt or closer to the DSB was DNA MMR independent, irrespective of the ssODN half instructing the mutation. In contrast, induction of a mutation 15 nt from the break and instructed by the 3′ half of the ssODN, profited from DNA MMR. Consistent with the effect of MMR, we found that replacement of the mismatching DNA nucleotide at position +15 for a mismatching LNA (analogous to Figure 2E, insert) decreased the mutation efficiency in MMR-proficient Hap1 cells approximately 4-fold (Figure 2G, insert). Induction of mutations somewhat further downstream was low in both MMR-proficient and -deficient cells. Also, in human MMR-proficient RPE-cells but not in *Mlh1*-deficient 293FT cells, we could efficiently introduce a mutation from the 3′ half of the ssODN. (Supplementary Figure S7). Although in Hap1 cells the effect of MMR was restricted to one position (+15), together these results demonstrate that induction of mutations from the 3′ half of the ssODN can be problematic in MMR-defective human cells.

Next, we investigated whether mutations could be introduced even further away from the DSB. We designed 120 nt ssODN templates to create an ATG 42 bp downstream from the break (Figure 3A, design A). In mESCs, introduction of the mutation from the 3′ half (the sense oligonucleotides), but not from the 5′ half (the anti-sense oligonucleotides) was MSH2 dependent (Figure 3B). Since the mutating nucleotide is now closer to the ssODN end, we tested whether the inhibition of end-degradation of the ssODN through incorporation of phosphorothioate (PTO) linkages could increase gene-editing efficiencies. When the mutation was introduced from the 3′ half of the ssODN, PTO linkages at this end raised the targeting efficiency from 2 to 6% (Figure 3B). Protecting the opposite end had no effect. Neither 5′ nor 3′ PTO protection increased substitution efficiencies when the mutating nucleotide was in the 5′ half (Figure 3B). Thus, degradation of the 3′-ends of ssODNs impaired introduction of distal substitutions from the 3′ end. Extending the ssODN at the 3′ end increased the substitution efficiency as well. However, also with an extended 3′ end, gene editing still profited from 3′ end protection by PTOs (Figure 3A and B, design B). No effect of 5′ or 3′ ssODN PTO protection was seen when the mutating nucleotide was positioned in close proximity of the DSB and 61 nt from the 3′ end (at variance with a previous report (23)) (Supplementary Figure S5a and b). For a mutation 15 nt from the break and 27 nt from the 3′ end, PTO protection increased the introduction efficiency to the level of break-proximal mutation efficiencies (Supplementary Figure S5c and d).

The results obtained with our reporter system propose a protocol for effective introduction of base substitutions distal from a CRISPR/Cas9-induced DSB that relies on DNA MMR and the use of 3′-end protected oligonucleotides. We finally investigated whether this protocol enables introduction of DSB distal mutations in mESCs at other endogenous chromosomal loci as well. We designed gRNAs targeting mouse *Msh2*, *Msh6* and *Mlh1* genes and 120 nt long oligonucleotide templates that create two novel restriction sites; one in close proximity and a second 40–47 nt away from the DSB (Figure 4A). We tested sense and antisense versions to compare base-pair substitutions instructed by the 3′ and 5′ halves, respectively, and to study the effects of PTO protection and MMR activity. Introduction of a restriction site close to the break was efficient in

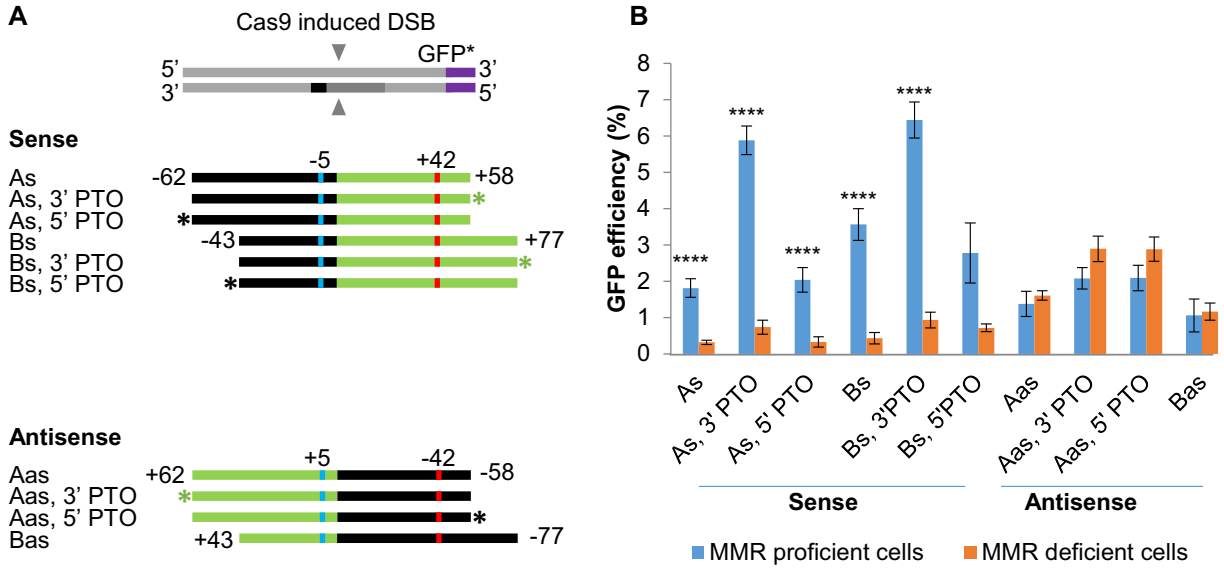

Figure 3. Effects of the end protection of oligonucleotides. (**A**) Introduction of a mutation at 42 nt from the break site using 120 nt ssODN templates. Red rectangles indicate single base-pair substitutions. Blue rectangles represent a PAM disrupting mutation. Asterisks at the ends denote double PTO linkages. Numbers above red and blue rectangles indicate their distance to the DSB site; numbers adjacent to the ssODNs indicate the distance of the end to the DSB. (**B**) Percentage of GFP-positive cells obtained with the templates in (**A**) ($n = 6$; stars above blue bars represent P-values determined between MMR-proficient and -deficient samples; ****$P < 0.0001$; P-value between ssODN As and As, 3'PTO in MMR deficient cells ≈ 0.07). Template oligonucleotides used in this study are shown in Supplementary Table S1.

MMR-proficient and *Msh2*-deficient cells (Figure 4B, left panels). In contrast, at all three loci, introduction of a restriction site distal from the break was most efficient when the mutation was present in the 3′ half of the ssODN, the 3′ end was PTO protected and the experiment was performed in MMR-proficient cells (Figure 4B, right panels). Notably, MMR promoted the introduction of 3′-half instructed mutations by PTO-protected ssODNs 8- to 9-fold, or even more (in case of *MSH2*). Furthermore, we found that break-distal mutations were always introduced simultaneously with break-proximal mutations on the same allele (Supplementary Figure S6).

DISCUSSION

Although ssODN templates are routinely used in nuclease-assisted knock-in protocols, the mechanism of ssODN-mediated DSB repair is not fully understood. The bridge model predicts incorporation of the ssODN into the genome, and has steps in common with single-strand annealing. In the template model, the ssODN serves as a template and does not become physically incorporated into the genome. The template model shares several processes with homologous recombination, such as 5′-end resection and ssODN-templated genomic 3′-end extension.

The two models make different predictions as to the introduction efficiency of mutations from the 5′ and 3′ halves of the ssODN (the halves separated by the projected break site by Cas9). In an MMR-deficient setting, DSB repair according to the bridge model would introduce mutations from both halves of the ssODN equally effectively, as the entire ssODN becomes incorporated into the genome. The template model, on the other hand, allows introduction of mutations only from the 5′ half of the ssODN. Our findings are in accordance with the latter prediction. Similarly, several recent reports provided support for the template mechanism of DSB repair by studying simultaneous introduction of a selectable break-proximal mutation and silent break-distal mutations in MMR-deficient cells (9,10). For example, Kan *et al.* used single-stranded donor DNA oligonucleotides instructing six extra silent mutations (single-nucleotide polymorphisms, SNPs), three on either side of the break-proximal mutation that converted enhanced green fluorescent protein (EGFP) to blue fluorescent protein (BFP) (10). Consistent with our results and an earlier observation of Davis and Maizels (9), SNP retention in BFP-expressing cells obtained after DSB repair showed a strong bias: in MMR-deficient HCT116 cells, SNPs present on the 5′ side of the ssODN were incorporated with higher frequency than 3′-side-located SNPs. Also during *nick repair* using ssODN donors complementary to the nicked strand (cN), the preferred incorporation of 5′-side over 3′-side polymorphisms is supportive of the template model (9,10). However, these findings may not exclude the bridge mode if the ssODN is subject to extensive 3′-end degradation: this would preclude effective introduction of 3′-half-instructed mutations also in the bridge model. We consider this possibility unlikely as we found that 3′-end-protection by PTO linkages only modestly increased the introduction efficiency of 3′-half-instructed mutations in MMR-deficient cells (compare As and As 3'PTO, Figure 3B, P-value 0.07), which remained much lower than the introduction efficiency of 5′-half-instructed mutations (Aas 3'PTO, Figure 3B).

Kan *et al.* also reported that during nick repair, MMR reduced the efficiency of ssDI (incorporation of an ssODN complementary to the intact strand) as well as the size of conversion tracts during SDSA repair (the ssODN is com-

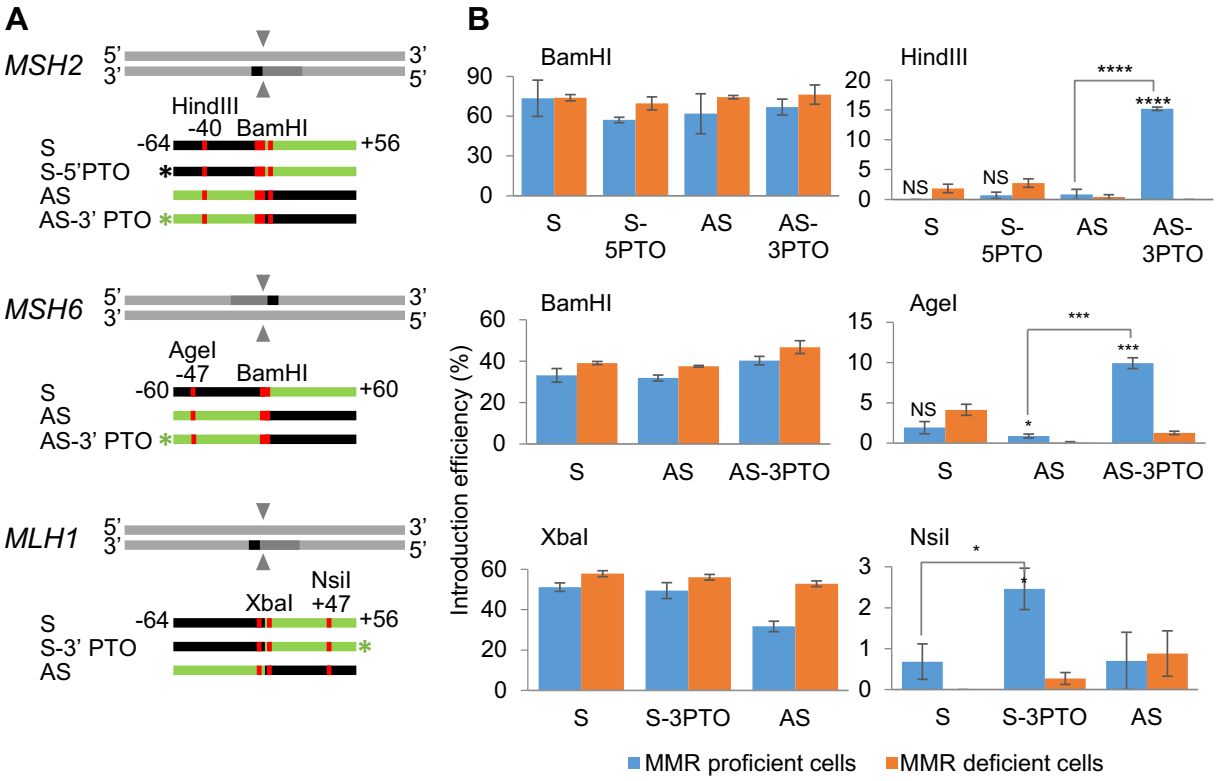

Figure 4. Efficiency of break-distal versus break-proximal substitutions at three endogenous genes. (**A**) Introduction of break-proximal and break-distal restriction sites at three endogenous genomic loci (represented by light gray lines). Indicated are the PAM (black) and the protospacer (dark gray) regions. Sense (S) and antisense (AS) ssODNs are divided in 5′ (black) and 3′ (green) halves. Red rectangles indicate the position of mutating nucleotides. Compound mutations no more than 3 bp from the break site create a BamHI, BamHI or XbaI site in the *Msh2*, *Msh6* or *Mlh1* genes, respectively. A single base pair mutation induces a HindIII, AgeI or NsiI site, respectively, further from the break. Asterisks indicate PTO linkages. Numbers beneath restriction sites indicate their distance to the DSB site, numbers adjacent to the oligonucleotides indicate the distance of the ends to the DSB. (**B**) Percentages of restriction site cleavage. The CRISPR/Cas9-ssODN-modified loci were amplified by PCR on gDNA and subsequently digested with the indicated restriction enzymes. Amounts of cleaved and uncleaved DNA were quantified by the Labchip Caliper GX. Stars above blue bars represent *P*-values determined between MMR-proficient and -deficient samples; $****P < 0.0001$, $***P < 0.001$, $**P < 0.01$, $*P < 0.05$). Three representative Caliper plots are shown in Supplementary Figure S8, produced with gDNA from MMR-proficient mESCs from Figure 2B transfected with the *Msh2* gRNA and the AS-3' PTO ssODN.

plementary to the nicked strand and used as a template), which they interpreted as indicative for MMR-dependent heteroduplex rejection (10). The latter contrasts to our results that would predict an extension rather than contraction of co-conversion tracts at the 3′ side of the ssODN. This discrepancy may be related to critical differences between ssODN-directed nick repair and DSB repair, but the latter was not studied in MMR-proficient cells by Kan *et al*. (10). However, incorporation of distal 5′ and 3′ SNPs during DSB repair in MMR-proficient human iPS cells was studied by Yang *et al*. and found to be equally effective, consistent with our results (24). Thus, our observation that incorporation of 3′-located distal mutations is promoted by DNA MMR reconciles several earlier observations spread over different publications. We propose this critical role of MMR can be best explained by the template model of DSB repair as depicted in Figure 5A. Although a mismatch created by annealing of the 3′ half of the ssODN may frequently elicit MMR-dependent heteroduplex rejection, the high concentration of ssODN may ultimately drive extension of the annealed 3′ gDNA end, thus stabilizing the interaction with the ssODN. Now, a canonical MMR reaction can take place leading to degradation of part of the genomic 3′ single-stranded end. Subsequent DNA synthesis can now copy the mutation instructed by the 3′ half of the ssODN into the genome. Our observation that introduction of 3′-instructed mutations benefits from 3′-end protection by PTO linkages is consistent with the template model: PTO protection of the ssODN 3′ end ensures sufficient oligonucleotide sequence remains available for heteroduplex formation and subsequent MMR action (Figure 5B).

A recent study on break-induced replication (BIR) in yeast may provide a precedent for such activity of MMR where it appeared necessary for copying information located upstream of the invading genomic 3′ end from a double-stranded template (25). Our finding that introduction of 3′-half-instructed mutations in close vicinity to the break site was largely MMR independent and similarly effective as 5′-half-instructed break-proximal mutations, likely indicates some erosion of the 3′ gDNA ends removing the sequence that would otherwise create a mismatch upon annealing to the ssODN. This is supported by a study by Dorsett *et al*. who investigated the structure of DNA ends produced by Cas9 with nucleotide resolution and found the majority to lack several terminal nucleotides (26). The yeast study on BIR cited above suggested a role for

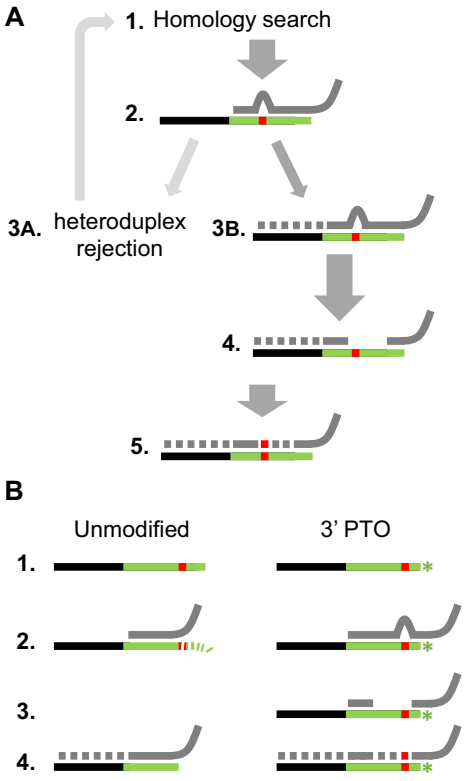

Figure 5. Models for ssODN-templated DSB repair. (**A**) Proposed role of MMR during ssODN-templated DSB repair. **1.** Homology search is performed by the 3′ gDNA. **2.** The gDNA anneals to the ssODN template, creating a mismatch at the position of the planned substitution (indicated by red rectangle). **3A.** The mismatch may elicit MMR-mediated heteroduplex rejection returning the reaction to step **1. 3B.** Intermediate 2 may be stabilized by extension of the 3′ genomic end by DNA polymerase using the ssODN as template. **4.** Post-replicative DNA MMR may now remove part of the genomic sequence around the mismatch and copy the ssODN-instructed alteration into the genome (**5**). (**B**) Benefit of 3′ end PTO protection for introduction of break distal mutations. **1.** The mutation is placed close to the 3′ end of the ssODN. **2.** This end is subject to degradation, precluding annealing around the mismatching nucleotide. In case of 3′ PTO end protection (asterisk), a heteroduplex can be formed. **3.** The mismatch elicits MMR to degrade part of the 3′ gDNA end. **4.** Elongation of the gDNA does not result in incorporation of the mutation in case the ssODN 3′ end is unprotected; in case of a protected 3′ end, the mutation instructed by the ssODN is copied into the genome.

exonucleolytic 3′-to-5′ proofreading activity of DNA polymerase δ in the degradation of the 3′ gDNA end (25).

Erosion of 3′ genomic ends also implies that break-proximal mutations are simultaneously introduced into both gDNA strands. In contrast, 5′ half instructed break-distal mutations are initially introduced into only one strand, and according to the template model, result in a heteroduplex upon re-annealing of the 3′ gDNA ends (see Supplementary Figure S1b, step 4). The subsequent heteroduplex resolution results in a maximum theoretical mutation-introduction efficiency 2-fold lower than that of break-proximal mutations: in MMR-proficient cells the heteroduplex may be targeted by canonical MMR, either converting the mutation to the other gDNA end or removing it and restoring the wild-type situation; in DNA MMR-deficient cells, replication will produce one daughter cell with and one without the mutation. On the other hand, the theoretical maximum of the introduction efficiency of break-distal mutations instructed by the 3′ half equals that of break-proximal mutations. Nonetheless, we did observe lower efficiencies (Figure 2). Reduced efficiencies are likely the result of 3′ end degradation of the ssODN, impairing heteroduplex formation and hence MMR-dependent mutation incorporation. Indeed, if the 3′ end of an ssODN instructing a mutation from the 3′ half at position +15 was protected against degradation by PTO linkages, we observed the +15 mutation was introduced with the same efficiency as break proximal mutations (Supplementary Figure S5d). At variance with Renaud *et al*. (23), we found that only break-distal but not break-proximal substitutions benefited from PTO end protection. Possibly, the extent of 3′ end degradation of ssODNs is cell-type dependent. In murine ESCs, end degradation may be relatively moderate only affecting 3′-end-proximal nucleotides.

While PTO end-protection promoted templated repair of a Cas9-induced DSB (our results, ref. 23), we and others previously reported that PTO-containing ssODNs performed less well in a gene modification protocol *without* the assistance of site-specific nucleases (15,16,19). We believe there are two explanations for the differential toxicity of PTO linkages between ssODN-mediated gene modification protocols with and without the assistance of site-specific nucleases. First, the amount of ssODNs entering the cell is likely to be much higher in protocols that do not use nucleases, however, we have no direct proof for this. A second, more appealing explanation is that the mechanisms of gene modification differ. We and others have provided evidence that without targeted nucleases, oligonucleotides incorporate into the replication fork and physically become part of the modified genome (19,27). In contrast, ample evidence exists (our present work, refs. 8–10) that during double-stranded break repair, the oligonucleotide only serves as a template and does not physically integrates into the genome. It is therefore conceivable that PTO-containing ssODNs only confer toxicity when they become introduced into the genome. Although we have no direct evidence for toxicity of genomic PTOs, this view is supported by our previous observation that modified cells obtained with PTO-containing ssODNs (but without nuclease assistance) showed a marked proliferative disadvantage compared to non-modified cells (19).

The model depicted in Figure 5 is largely based on observations in mouse ESCs. To study its general applicability, we performed experiments in human cells. By comparing an isogenic set of MMR-proficient and -deficient Hap1 cells, we found that MMR promoted the transfer of genetic information from the 3′ half of the ssODN only at a single position (+15), as evidenced by two independent observations: (i) in MMR-deficient cells, the efficiency was significantly lower than in MMR-proficient cells ($P < 0.001$); (ii) An LNA at this position (rendering the mismatch invisible to the MMR system) significantly reduced the efficiency in MMR-proficient cells ($P < 0.0001$). Both observations demonstrate the stimulating effect of MMR at position +15. Why then no effect at other positions? One explanation may be that in Hap1 cells single-stranded ends (both genomic and oligonucleotide 3′ ends) are more susceptible

to degradation than in ES cells. For example, the +9/+10 mutation could not efficiently be instructed by the 3′-half of the ssODN in MMR-deficient mESCs while it was in Hap1 cells (Figure 2G), indicating that in Hap1 cells genomic 3′ end erosion extended to 10 nt from the break. Similarly, the low efficiency of +18/+21 mutations may be indicative for 3′ end degradation of the oligonucleotide. Consistent with an effect of MMR in human cells, an MMR-proficient and -deficient cell line showed a marked difference in co-conversion of a 3′-located break-distal mutation. Admittedly, these cell lines were not isogenic and hence caution is needed to interpret these results as additional proof for the applicability of our model in human cells. Nonetheless, our observations may provide a warning to users of common MMR-defective human cell lines (like 293T or HCT116): the absence of MMR may preclude effective introduction of break-distal mutations. Our studies in ESCs and Hap1 cells provide a possible explanation: the requirement for MMR to ensure copying the 3′ half of the oligonucleotide template.

In summary, effective break-distal base-pair substitution, instructed by the 3′ half of oligonucleotides requires MMR in mouse ESCs and possibly in human cell lines as well. Furthermore, PTO protection of the 3′ ssODN end enables substitutions as far as 47 nucleotides from the break site. These findings guide the design of gene editing strategies at sites for which no suitable proximal nuclease is available.

DATA AVAILABILITY

The sequences presented in Supplementary Notes 1 and 2 are deposited to GenBank:

PGKpur: KX548903; GFP reporter cassette: KX548904.

SUPPLEMENTARY DATA

Supplementary Data are available at NAR Online.

ACKNOWLEDGEMENTS

We acknowledge support from the NKI flow cytometry and sequencing core facilities. We thank our colleagues Bente Benedict, Marleen Dekker, Heinz Jacobs, Thomas van Ravesteyn and Joey Riepsaame for helpful discussions and comments on the manuscript and Marleen Dekker for technical assistance.

FUNDING

The Netherlands Organization for Health Research and Development [ZonMw-TOP 40–00812-98–10033]. Funding for open access charge: The Netherlands Cancer Institute.

Conflict of interest statement. None declared.

REFERENCES

1. Jinek,M., Chylinski,K., Fonfara,I., Hauer,M., Doudna,J.A. and Charpentier,E. (2012) A programmable dual-RNA-guided DNA endonuclease in adaptive bacterial immunity. *Science*, **337**, 816–822.
2. Cong,L., Ran,F.A., Cox,D., Lin,S., Barretto,R., Habib,N., Hsu,P.D., Wu,X., Jiang,W., Marraffini,L.A. *et al.* (2013) Multiplex genome engineering using CRISPR/Cas systems. *Science*, **339**, 819–823.
3. Mali,P., Yang,L., Esvelt,K.M., Aach,J., Guell,M., DiCarlo,J.E., Norville,J.E. and Church,G.M. (2013) RNA-guided human genome engineering via Cas9. *Science*, **339**, 823–826.
4. Orlando,S.J., Santiago,Y., DeKelver,R.C., Freyvert,Y., Boydston,E.A., Moehle,E.A., Choi,V.M., Gopalan,S.M., Lou,J.F., Li,J. *et al.* (2010) Zinc-finger nuclease-driven targeted integration into mammalian genomes using donors with limited chromosomal homology. *Nucleic Acids Res.*, **38**, 1–15.
5. Radecke,S., Radecke,F., Cathomen,T. and Schwarz,K. (2010) Zinc-finger nuclease-induced gene repair with oligodeoxynucleotides: wanted and unwanted target locus modifications. *Mol. Ther.*, **18**, 743–753.
6. Storici,F., Snipe,J.R., Chan,G.K., Gordenin,D.A. and Resnick,M.A. (2006) Conservative repair of a chromosomal single-strand DNA through two steps of annealing. *Mol. Cell. Biol.*, **26**, 7654–7657.
7. Kowalczykowski,S.C. (2015) An overview of the molecular mechanisms of recombinational DNA repair. *Cold Spring Harb. Perspect. Biol.*, **7**, a016410.
8. Davis,L. and Maizels,N. (2014) Homology-directed repair of DNA nicks via pathways distinct from canonical double-strand break repair. *Proc. Natl. Acad. Sci. U.S.A.*, **111**, 924–932.
9. Davis,L. and Maizels,N. (2016) Two distinct pathways support gene correction by single stranded donors at DNA nicks. *Cell. Rep.*, **17**, 1872–1881.
10. Kan,Y., Ruis,B., Takasugi,T. and Hendrickson,E.A. (2017) Mechanisms of precise genome editing using oligonucleotide donors. *Genome Res.*, **27**, 1099–1111.
11. de Wind,N., Dekker,M., Berns,A., Radman,M. and te Riele,H. (1995) Inactivation of the mouse Msh2 gene results in mismatch repair deficiency, methylation tolerance, hyperrecombination, and predisposition to cancer. *Cell*, **82**, 321–330.
12. Dekker,M., Brouwers,C. and te Riele,H. (2003) Targeted gene modification in mismatch-repair-deficient embryonic stem cells by single-stranded DNA oliogonucleotides. *Nucleic Acids Res.*, **31**, e27.
13. Aarts,M., Dekker,M., De Vries,S., Van der Wal,A. and te Riele,H. (2006) Generation of a mouse mutant by oligonucleotide-mediated gene modification in ES cells. *Nucleic Acids Res.*, **34**, e147.
14. Olsen,P.A., Solhaug,A., Booth,J.A., Gelazauskaite,M. and Krauss,S. (2009) Cellular responses to targeted genomic sequence modification using single-stranded oligonucleotides and zinc-finger nucleases. *DNA Repair*, **8**, 298–308.
15. Papaioannou,I., Disterer,P. and Owen,J.S. (2009) Use of internally nuclease-protected single-strand DNA oligonucleotides and silencing of the mismatch repair protein, MSH2, enhances the replication of corrected cells following gene editing. *J. Gene Med.*, **11**, 267–274.
16. Rios,X., Briggs,A.W., Christodoulou,D., Gorham,J.M., Seidman,J.G. and Church,G.M. (2012) Stable gene targeting in human cells using single-strand oligonucleotides with modified bases. *PLoS One*, **7**, e36697.
17. Carette,J.E., Raaben,M., Wong,A.C., Herbert,A.S., Obernosterer,G., Mulherkar,N., Kuehne,A.L., Kranzusch,P.J., Griffin,A.M., Ruthel,G. *et al.* (2011) Ebola Virus entry requires the cholesterol transporter Niemann-Pick C1. *Nature*, **477**, 340–343.
18. Irion,S., Luche,H., Gadue,P., Fehling,H.J., Kennedy,M. and Keller,G. (2007) Identification and targeting of the *ROSA26* locus in human embryonic stem cells. *Nat. Biotechnol.*, **25**, 1477–1482.
19. Aarts,M. and te Riele,H. (2010) Subtle gene modification in mouse ES cells: evidence for incorporation of unmodified oligonucleotides without induction of DNA damage. *Nucleic Acids Res.*, **38**, 6956–6967.
20. Paquet,D., Kwart,D., Chen,A., Sproul,A., Jacob,S., Teo,S., Olsen,K.M., Gregg,A., Noggle,S. and Tessier-Lavigne,M. (2016) Efficient introduction of specific homozygous and heterozygous mutations using CRISPR/Cas9. *Nature*, **533**, 125–129.
21. van Ravesteyn,T.W., Dekker,M., Fish,A., Sixma,T.K., Wolters,A., Dekker,R.J. and te Riele,H.P.J. (2016) LNA modification of single-stranded DNA oligonucleotides allows subtle gene modification in mismatch-repair-proficient cells. *Proc. Natl. Acad. Sci. U.S.A.*, **113**, 4122–4127.
22. Modrich,P. (2016) Mechanisms in *E. coli* and human mismatch repair (nobel lecture). *Angew. Chem. Int. Ed. Engl.*, **55**, 8490–8501.
23. Renaud,J.B., Boix,C., Charpentier,M., De Cian,A., Cochennec,J., Duvernois-Berthet,E., Perrouault,L., Tesson,L., Edouard,J., Thinard,R. *et al.* (2016) Improved genome editing efficiency and

flexibility using modified oligonucleotides with TALEN and CRISPR-Cas9 nucleases. *Cell Rep.*, **14**, 2263–2272.
24. Yang,L., Guell,M., Byrne,S., Yang,J.L., De Los Angeles,A., Mali,P., Aach,J., Kim-Kiselak,C., Briggs,A.W., Rios,X. *et al.* (2013) Optimization of scarless human stem cell genome editing. *Nucleic Acids Res.*, **41**, 9049–9061.
25. Anand,R., Beach,A., Li,K. and Haber,J. (2017) Rad51-mediated double-strand break repair and mismatch correction of divergent substrates. *Nature* **544**, 377–380.
26. Dorsett,Y., Zhou,Y., Tubbs,A.T., Chen,B.R., Purman,C., Lee,B.S., George,R., Bredemeyer,A.L., Zhao,J.Y., Sodergen,E. *et al.* (2014) HCoDES reveals chromosomal DNA end structures with single-nucleotide resolution. *Mol. Cell.* **56**, 808–818.
27. Radecke,S., Radecke,F., Peter,I. and Schwarz,K. (2006) Physical incorporation of a single-stranded oligodeoxynucleotide during targeted repair of a human chromosomal locus. *J. Gene Med.*, **8**, 217–228.